

# High-resolution Spaceborne SAR Processing Using the Decomposed Transfer Function

**KNUT ELDHUSET**

Norwegian Defence Research Establishment (FFI),

Air and Space Systems Division, PO Box 25, 2027 Kjeller, Norway

Phone:+47-63807478 Fax: +47-63807212

Email: [Knut.Eldhuset@ffi.no](mailto:Knut.Eldhuset@ffi.no)

**Abstract:** In this paper a new analytic decomposed transfer function (DTF) for spaceborne SAR (Synthetic Aperture Radar) processing is calculated using the stationary phase approximation and Taylor's series expansion. The DTF copes with large Doppler centroid variations and executes range cell migration correction, secondary range compression, azimuth compression and higher order effects. A fourth-order (DTF4) and a fifth-order (DTF5) algorithm have been implemented using segmented block processing. It is shown that the DTF4 yields high quality 3-look target responses at azimuth resolution 0.3 m and range resolution 0.5 m at low squint ( $\text{yaw}=0.3^\circ$ ) for X-band. At higher squint ( $\text{yaw}=7.5^\circ$ ) the DTF5 has to be used to obtain adequate image quality.

## I. INTRODUCTION

In [1] it was stated that the hyperbolic phase history used for airborne SAR is not sufficient for processing of spaceborne SAR data with azimuth resolution of some decimeters. This was later confirmed by several papers [2,3,4]. The EETF4 (Extended Exact Transfer Function fourth-order) algorithm was originally developed in [5] using the stationary phase approximation (SPA) for calculation of the 2-D transfer function. The azimuth filter in this algorithm has recently been selected for KOMPSAT-6 SAR processing [6]. In [7] the EETF4 was adapted to spaceborne bistatic SAR processing. The EETF4 algorithm was able to cope with range variations in the Doppler parameters, however, some degradation was

observed with increasing squint because of invariable parameters for the range cell corrections within one block. The EETF4 algorithm was not decomposed as they did in [8] where the 2-D transfer function of fourth-order was elegantly decomposed in components that identify the azimuth modulation (AZ), range cell migration (RCM), the secondary range cell migration (SRC) and higher order terms (residual phase) (HIGH). In the algorithm in [8], a fourth-order phase history based on the sum of two hyperbolic phase histories was introduced for a bistatic SAR. They used the method of series reversion (MSR) to calculate the stationary point instead of solving polynomial equations as we do in this paper. In [9] they combined the Doppler range model from [5] and the MSR from [8] to avoid complicated expressions for the exact transfer function. In this approach they assume small Doppler centroids and variations in range. In [2] they propose a velocity scaling algorithm (VSA) which performs better than the traditional hyperbolic range model. They ignore the third- and fourth-order terms when they do the stationary phase approximation. Another approach for processing very high resolution spaceborne SAR was presented in [4]. They use a numerical approach resembling the motion compensation for airborne SAR in order to cope with non-hyperbolic azimuth phase history.

Most of the algorithms developed for very high resolution SAR assume that the platform is yaw steered and assume a small Doppler centroid and a slight variation over range. In [10] they compared three well known algorithms: the range-Doppler algorithm (RDA) [11], the chirp-scaling algorithm (CSA) [12] and the monochromatic wavenumber-

domain algorithm (MWA) [13]. They found that the MWA was a good candidate for block processing when the Doppler centroid variation over range is large.

The algorithm proposed here uses fourth-order and fifth-order azimuth phase history and solves analytically polynomial equations to calculate the 2-D transfer function. We decompose the phase function by Taylor's series expansion of the stationary point solution. We identify the same components in the decomposed function as they did in [8], and we call the algorithm the Decomposed Transfer Function of fourth-order (DTF4) and fifth-order (DTF5). The 2-D transfer function is calculated as in [5] for the fourth-order azimuth phase history and for the fifth-order phase history in a similar way. In the last case a fourth-order equation has to be solved instead of a third-order equation in each point. The expressions for the transfer function are more complex than for most of the algorithms in the literature, however, the ability to process azimuth resolution down to 10 cm or 3-look 30 cm resolution and block processing with large Doppler centroid variations should be an advantage. The algorithm may be well suited for parallel computing and has been implemented with 8 cores using OpenMP library in Windows. However, an analysis of the computational efficiency has so far not been done. The DTF4 or DTF5 could be implemented for staring spotlight processing of TerraSAR-X data where non-hyperbolic phase history may be needed [4].

This paper is organized as follows. In Section IIA the Exact Transfer Function from [5] is briefly reviewed. The calculation of the DTF4 is shown in Section IIB. In Section IIC the calculation of the fifth-order ETF is done and the calculation of DTF5 is shown in Section IID. We present the implementation by showing the flow diagram of the algorithm in Section IIE. Simulation examples and the achieved performance of the DTF algorithm are given in Section III. Finally, in Section IV novel properties of the algorithm are compared with other state-of-the-art algorithms.

## II FOURTH-ORDER AND FIFTH-ORDER DTF ALGORITHM

### A. Exact Transfer Function (ETF)

If we omit some constants the exact transfer function (ETF) can be written as in (38) in [5]

$$H_{ETF}(\omega_r, \omega_a; R) = \mathbb{F}_r \left\{ \exp \left[ j\Phi_r(t_r) \right] \right\} \exp \left[ j\varphi(t_a^*) \right] \quad (1)$$

$\mathbb{F}_r \left\{ \exp \left[ j\Phi_r(t_r) \right] \right\}$  is the Fourier transform of the transmitted signal and  $t_r$  is the range time.  $R$  is slant range and the phase function  $\varphi(t_a^*)$  in (1) is evaluated at the stationary point solution  $t_a^*$

$$\varphi(t_a^*) = 2R(t_a^*) \left( \frac{2\pi}{\lambda} - \frac{\omega_r}{c} \right) - \omega_a t_a^* \quad (2)$$

where  $R(t_a)$  is the range migration as a function of the azimuth time  $t_a$ .  $\omega_a$  and  $\omega_r$  are the azimuth and range frequency, respectively. In (2) there is a minus sign in the parenthesis instead of a plus sign as in [5].  $c$  is the speed of light and  $\lambda$  is the radar wavelength. In [8] they decomposed the phase function in the 2-D spectrum. To better understand the decompositions to be derived below the reader may review page 16 in [8]. In a similar way we decompose the azimuth phase function  $\varphi(t_a^*)$  above in the following manner

$$\begin{aligned} \varphi_{DTF}(t_a^*) &= kC_{00} + \varphi_{AZ}(\omega_a) + \varphi_{RM}(\omega_r, \omega_a) + \\ &\varphi_{SRC}(\omega_r, \omega_a) + \varphi_{HIGH}(\omega_r, \omega_a) \end{aligned} \quad (3)$$

where  $k = \frac{2\pi}{\lambda}$  and  $C_{00}$  is a constant which shall be defined later.  $\varphi_{AZ}(\omega_a)$  is the azimuth modulation term,  $\varphi_{RM}(\omega_r, \omega_a)$  represents the range cell migration,  $\varphi_{SRC}(\omega_r, \omega_a)$  is the secondary range cell migration and the last term  $\varphi_{HIGH}(\omega_r, \omega_a)$  represents higher order terms. We shall in this paper decompose the phase function in (3) with fourth-order and fifth-order azimuth phase histories.

### B. Calculation of Fourth-Order DTF

If we model the range migration  $R(t_a)$  with a polynomial function in (2), the phase function in the fourth-order ETF can be written

$$\varphi_{ETF4}(t_a^*) = 2 \left( c_1 t_a^* + c_2 (t_a^*)^2 + c_3 (t_a^*)^3 + c_4 (t_a^*)^4 \right) \cdot \left( \frac{2\pi}{\lambda} - \frac{\omega_r}{c} \right) - \omega_a t_a^* \quad (4)$$

where  $c_1, c_2, c_3$  and  $c_4$  are parameters defined in (10). We decompose this phase function as

$$\varphi_{DTF4}(t_a^*) = kC_{00} + \varphi_{AZ4}(\omega_a) + \varphi_{RCM4}(\omega_r, \omega_a) + \varphi_{SRC4}(\omega_r, \omega_a) + \varphi_{HIGH4}(\omega_r, \omega_a) \quad (5)$$

and write the DTF4 as

$$H_{DTF4}(\omega_r, \omega_a; R) = \mathbb{F}_r \left\{ \exp \left[ j\Phi_r(t_r) \right] \right\} \cdot \exp \left[ j\varphi_{DTF4}(t_a^*) \right] \quad (6)$$

We insert (5) into (6) and get

$$H_{DTF4}(\omega_r, \omega_a; R) = \mathbb{F}_r \left\{ \exp \left[ j\Phi_r(t_r) \right] \right\} \cdot \exp \left[ j \left( kC_{00} + \varphi_{AZ4}(\omega_a) + \varphi_{RCM4}(\omega_r, \omega_a) + \varphi_{SRC4}(\omega_r, \omega_a) + \varphi_{HIGH4}(\omega_r, \omega_a) \right) \right] \quad (7)$$

The sum of the of the decomposed phase functions in the  $\exp$  function in (7) appears as a product of decomposed transfer functions

$$H_{DTF4}(\omega_r, \omega_a; R) = \exp(-j\omega_r^2 / 2b_2) \exp(jkC_{00}) \cdot \left[ H_{AZC4}(\omega_a; R) \cdot H_{RCM4}(\omega_r, \omega_a; R) \cdot H_{SRC4}(\omega_r, \omega_a; R) \cdot H_{HIGH4}(\omega_r, \omega_a; R) \right] \quad (8)$$

In (8) we have also used a linear chirp with rate  $b_2$  as the transmitted signal in (7).

Now we shall find the expression for the different terms in the fourth-order decomposed function. Then we must find the stationary point of derivative of (4) using the azimuth time  $t_a$

$$2 \left( c_1 + 2c_2 t_a + 3c_3 t_a^2 + 4c_4 t_a^3 \right) \cdot \left( \frac{2\pi}{\lambda} - \frac{\omega_r}{c} \right) - \omega_a = 0 \quad (9)$$

where

$$c_1 = -\frac{\lambda}{2} a_1 \quad c_2 = -\frac{\lambda}{2} a_2 \quad c_3 = -\frac{\lambda}{2} a_3 \quad c_4 = -\frac{\lambda}{2} a_4 \quad (10)$$

$a_1$  is the Doppler centroid,  $a_2$  is the Doppler frequency rate,  $a_3$  is the third Doppler parameter and,  $a_4$  is the fourth Doppler parameter. Assume that  $q^2 + p^3 < 0$ , then there are three stationary point solutions ((66-68) in [5])

$$t_a^* = y_\delta - \frac{c_3}{4c_4} \quad (11)$$

where  $\delta = 0, \frac{\pi}{3}$  or  $-\frac{\pi}{3}$  and

$$y_\delta = 2\sqrt{-p} \cos \left[ \frac{1}{3} \cos^{-1} \left( -(-p)^{\frac{3}{2}} \cdot q \right) + \delta \right] \quad (12)$$

We introduce a variable  $x$  defined by

$$x = -(-p)^{\frac{3}{2}} \cdot q \quad (13)$$

where  $p$  and  $q$  are given in (63, 64) in [5])

$$p = -\frac{1}{16} \left( \frac{c_3}{c_4} \right)^2 + \frac{1}{6} \frac{c_2}{c_4} \quad (14)$$

$$q = \frac{c_1}{8c_4} + \frac{1}{64} \left( \frac{c_3}{c_4} \right)^3 - \frac{1}{16} \frac{c_2 c_3}{c_4^2} - \frac{\omega_a}{16c_4} \left( \frac{2\pi}{\lambda} - \frac{\omega_r}{c} \right) \quad (15)$$

We approximate  $x$  as

$$x = p_2 q_1 + p_2 q_2 \omega_a + \frac{p_2 q_2}{ck} \omega_r \omega_a \quad (16)$$

where

$$q_1 = \frac{c_1}{8c_4} + \frac{1}{64} \left( \frac{c_3}{c_4} \right)^3 - \frac{1}{16} \frac{c_2 c_3}{c_4^2} \quad (17)$$

$$q_2 = -\frac{\lambda}{32\pi c_4} \quad (18)$$

$$p_2 = -(-p)^{3/2} \quad (19)$$

For  $q^2 + p^3 > 0$  the solution is given by Cardano's formula ((65) in [5]) instead of (12). We omit the calculations here. We take the third derivative of (12) and take a third-order Taylor's series expansion of  $y_\delta$

$$y_\delta(x) = y_0 + y_1(x - x_m) + \frac{1}{2} y_2(x - x_m)^2 + \frac{1}{6} y_3(x - x_m)^3 \quad (20)$$

We define a point  $x_m$  where the Taylor polynomial is generated

$$x_m = (x_{\max} + x_{\min}) / 2 \quad (21)$$

where  $x_{\max}$  and  $x_{\min}$  are the min and max values of  $x$ . The coefficients of (20) are then given by

$$y_0 = y_\delta(x_m) = p_1 \cos \left[ \frac{1}{3} \cos^{-1}(x_m) + \delta \right] \quad (22)$$

$$y_1 = y_\delta^{\cdot}(x_m) = \frac{1}{3} p_1 \cos \left[ \frac{1}{3} \cos^{-1}(x_m) + \delta \right] (1-x_m)^{-\frac{1}{2}} \quad (23)$$

$$y_2 = y_\delta^{\cdot\cdot}(x_m) = \frac{1}{3} p_1 \left\{ \begin{array}{l} -\frac{1}{3} \cos \left[ \frac{1}{3} \cos^{-1}(x_m) + \delta \right] \cdot \\ (1-x_m^2)^{-1} + \\ \sin \left[ \frac{1}{3} \cos^{-1}(x_m) + \delta \right] \cdot \\ x(1-x_m^2)^{-\frac{3}{2}} \end{array} \right\} \quad (24)$$

$$y_3 = y_\delta^{\cdot\cdot\cdot}(x_m) = \frac{1}{3} p_1 (A'B + AB' + C'D + CD') \quad (25)$$

$$A' = \frac{1}{9} \sin \left[ \frac{1}{3} \cos^{-1}(x_m) + \delta \right] \left[ -(1-x_m^2)^{-\frac{1}{2}} \right] \quad (26)$$

$$B' = 2x(1-x_m^2)^{-2} \quad (27)$$

$$C' = (1-x_m^2)^{-\frac{3}{2}} - 3x(1-x_m^2)^{-\frac{5}{2}} \quad (28)$$

$$D' = \frac{1}{3} \cos \left[ \frac{1}{3} \cos^{-1}(x_m) + \delta \right] \left[ -(1-x_m^2)^{-\frac{1}{2}} \right] \quad (29)$$

If we put the approximation for  $x$  in (16) into (20) it can be shown that

$$y_\delta(x) = T_0 + T_1 \omega_a + T_2 \omega_r \omega_a + T_3 \omega_a^2 + T_4 \omega_r \omega_a^2 + T_5 \omega_r^2 \omega_a^2 + T_6 \omega_a^3 + T_7 \omega_r \omega_a^3 + T_8 \omega_r^2 \omega_a^3 + T_9 \omega_r^3 \omega_a^3 \quad (30)$$

We define  $x_1 = p_2 q_1$ ,  $x_2 = p_2 q_2$  and  $x_3 = \frac{p_2 q_2}{ck}$  and write (16) as

$$x = x_1 + x_2 \omega_a + x_3 \omega_r \omega_a \quad (31)$$

It can be shown that the  $T$  coefficients in (30) are given by the expressions in (70)-(79). We have found that we can omit some of the terms in (30) to obtain adequate image quality. We retain  $T_0, T_1, T_2, T_3, T_6$  and insert (30) into (11) and then insert (11) into (4). The phase function of the DTF4 can be written as (5)

$$\begin{aligned} \varphi_{DTF4}(t_a^*) &= kC_{00} + \varphi_{AZ4}(\omega_a) + \varphi_{RCM4}(\omega_r, \omega_a) + \\ &\varphi_{SRC4}(\omega_r, \omega_a) + \varphi_{HIGH4}(\omega_r, \omega_a) \end{aligned} \quad (32)$$

where the different terms are given by

$$\begin{aligned} \varphi_{AZ4}(\omega_r, \omega_a) &= (kC_{01} - T_0) \omega_a + (kC_{02} - T_1) \omega_a^2 + (kC_{03} - T_3) \omega_a^3 + \\ &(kC_{04} - T_6) \omega_a^4 + \sum_{n=5}^{12} kC_{0n} \omega_a^n \end{aligned} \quad (33)$$

$$\begin{aligned} \varphi_{RCM4}(\omega_r, \omega_a) &= \\ &\left[ (-c^{-1}C_{00}) + (kC_{11} - c^{-1}C_{01}) \omega_a + (kC_{12} - c^{-1}C_{02} - T_2) \omega_a^2 \right. \\ &\left. + \sum_{n=3}^{10} (kC_{1n} - c^{-1}C_{0n}) \omega_a^n - c^{-1} \sum_{n=11}^{12} (kC_{0n}) \omega_a^n \right] \omega_r \end{aligned} \quad (34)$$

$$\begin{aligned} \varphi_{SRC4}(\omega_r, \omega_a) &= \\ &\left[ (-c^{-1}C_{11}) \omega_a + \sum_{n=2}^8 (kC_{2n} - c^{-1}C_{1n}) \omega_a^n - c^{-1} \sum_{n=9}^{10} C_{1n} \omega_a^n \right] \omega_r^2 \end{aligned} \quad (35)$$

$$\begin{aligned} \varphi_{HIGH4}(\omega_r, \omega_a) &= \left[ (-c^{-1}C_{22}) \omega_a^2 + \right. \\ &\sum_{n=3}^6 (kC_{3n} - c^{-1}C_{2n}) \omega_a^n - c^{-1}C_{27} \omega_a^7 - c^{-1}C_{28} \omega_a^8 \left. \right] \omega_r^3 \\ &+ \left[ (-c^{-1}C_{33}) \omega_a^3 + (kC_{44} - c^{-1}C_{34}) \omega_a^4 - c^{-1}C_{35} \omega_a^5 - c^{-1}C_{36} \omega_a^6 \right] \omega_r^4 + \\ &\left[ (-c^{-1}C_{44}) \omega_a^4 \right] \omega_r^5 \end{aligned} \quad (36)$$

where (33) represents the azimuth modulation (AZ4) of the DTF4, (34) is the range cell migration (RCM4), (35) is the secondary range cell migration (SRC4) and (36) is higher order effects (HIGH4). The  $C_{mm}$  - coefficients are given by the expressions in (80)-(114).

### C. Calculation of the Fifth-Order ETF

The phase function of the fifth-order ETF is given by

$$\begin{aligned} \varphi_{ETF5}(t_a^*) &= \lambda \left( a_1 t_a^* + \frac{a_2}{2} (t_a^*)^2 + \frac{a_3}{3} (t_a^*)^3 + \frac{a_4}{4} (t_a^*)^4 + \frac{a_5}{5} (t_a^*)^5 \right) \\ &\left( \frac{2\pi}{\lambda} - \frac{\omega_r}{c} \right) - \omega_a t_a^* \end{aligned} \quad (37)$$

where  $a_5$  is the fifth Doppler parameter. We decompose this phase function as

$$\begin{aligned} \varphi_{DTF5}(t_a^*) &= kC_{00} + \varphi_{AZC5}(\omega_a) + \varphi_{RCM5}(\omega_r, \omega_a) + \\ &\varphi_{SRC5}(\omega_r, \omega_a) + \varphi_{HIGH5}(\omega_r, \omega_a) \end{aligned} \quad (38)$$

Now we shall find the expression for the different terms in the decomposed function of fifth-order. Then we must find the stationary point of the following equation

$$2\left(c_1 + 2c_2t_a + 3c_3t_a^2 + 4c_4t_a^3 + 5c_5t_a^4\right) \cdot \left(\frac{2\pi}{\lambda} - \frac{\omega_r}{c}\right) - \omega_a = 0 \quad \delta = 0, \frac{\pi}{3} \text{ or } -\frac{\pi}{3} \quad (48)$$

(39)

This is a fourth-order equation, and analytical solutions exist. The Norwegian mathematician Niels Henrik Abel proved in 1824 that the fifth-order polynomial equation has no general algebraic solution like the second-, third- and fourth-order equations, hence, if we want a sixth-order phase history, numerical methods must be used to solve a fifth-order equation if we want to find the stationary point. To solve the quartic equation in (39) we use the solution given in Wolfram Mathworld [14]. We rewrite (39) as

$$Z^4 + AZ^3 + BZ^2 + CZ + D = 0 \quad (40)$$

where we use  $Z$  as the unknown instead of  $t_a$  and define the coefficients

$$A = \frac{4c_4}{5c_5}, \quad B = \frac{3c_3}{5c_5}, \quad C = \frac{2c_2}{5c_5},$$

$$D = \frac{c_1}{5c_5} - \frac{\omega_a}{10c_5 \left(\frac{2\pi}{\lambda} - \frac{\omega_r}{c}\right)} \quad (41)$$

The quartic equation in (40) can be transformed to a cubic equation

$$Y^3 - BY^2 + (CA - 4D)Y + (4BD - C^2 - A^2D) = 0 \quad (42)$$

We define

$$a = 1, \quad b = -B, \quad c = (CA - 4D),$$

$$d = (4BD - C^2 - A^2D) \quad (43)$$

The solutions of the cubic equation in (42) are given by [15]

$$\text{If } 0 \leq q^2 + p^3$$

$$Y = u + v \quad (44)$$

$$u = \left[ -q + (q^2 + p^3)^{\frac{1}{2}} \right]^{\frac{1}{3}} \quad (45)$$

$$v = \left[ -q - (q^2 + p^3)^{\frac{1}{2}} \right]^{\frac{1}{3}} \quad (46)$$

$$\text{if } q^2 + p^3 < 0$$

$$Y = 2\sqrt{-p} \cos \left[ \frac{1}{3} \cos^{-1} \left( -(-p)^{-\frac{3}{2}} \cdot q \right) + \delta \right] \quad (47)$$

where

$$q = \frac{1}{27} \left( \frac{b}{a} \right)^3 - \frac{1}{6} \frac{bc}{a^2} + \frac{d}{2a} \quad (49)$$

$$p = -\frac{1}{9} \left( \frac{b}{a} \right)^2 + \frac{c}{3a} \quad (50)$$

The solutions of the quartic equation in (40) are then given by

$$Z_{1,2} = -\frac{1}{4}A + \frac{1}{2}R \pm \frac{1}{2}F \quad (51)$$

$$Z_{3,4} = -\frac{1}{4}A - \frac{1}{2}R \pm \frac{1}{2}E \quad (52)$$

$$R = \left( \frac{1}{4}A^2 - B - \frac{b}{3} + y \right)^{\frac{1}{3}} \quad (53)$$

where

$$y = Y - \frac{b}{3} \quad (54)$$

where  $Y$  is the solution of the cubic equation in (87) and

$$F = (F_1 + F_2 R^{-1})^{\frac{1}{2}} \quad (55)$$

$$E = (F_1 - F_2 R^{-1})^{\frac{1}{2}} \quad (56)$$

$$F_1 = \frac{3}{4}A^2 - R^2 - 2B \quad (57)$$

$$F_2 = \frac{1}{4}(4AB - 8C - A^3)R^{-1} \quad (58)$$

The minimum of the four solutions appear to be the physical reasonable solution for the stationary point

$$t_a^* = \min(Z_1, Z_2, Z_3, Z_4) \quad (59)$$

This solution is put into (37) to calculate the fifth-order ETF (ETF5). We have implemented an EETF5 algorithm in the same way as the EETF4 algorithm was implemented in [5].

#### D. Calculation of Fifth-Order DTF

We see from (41), (43), (49) and (50) that both  $p$  and  $q$  are functions of  $\omega_r$  and  $\omega_a$ . We insert the cubic solution (47) into (54) and expand a Taylor's series in two dimensions

$$\begin{aligned}
y &= y_{00} + y_{10}(q - q_0) + y_{01}(p - p_m) + y_{11}(q - q_m)(p - p_m) \\
&+ y_{20}(q - q_m)^2 + y_{02}(p - p_m)^2 + y_{30}(q - q_m)^3 + \\
&y_{03}(p - p_m)^3 + y_{21}(q - q_m)^2(p - p_m) + \\
&y_{12}(q - q_m)(p - p_m)^2
\end{aligned} \tag{60}$$

$$\begin{aligned}
y_{10} &= \left[ \frac{\partial y}{\partial q} \right]_{(q_m, p_m)} & y_{01} &= \left[ \frac{\partial y}{\partial p} \right]_{(q_m, p_m)} \\
y_{11} &= \left[ \frac{\partial^2 y}{\partial q \partial p} \right]_{(q_m, p_m)} & y_{01} &= \left[ \frac{\partial^2 y}{\partial p \partial q} \right]_{(q_m, p_m)}
\end{aligned} \tag{61}$$

$$\begin{aligned}
y_{30} &= \left[ \frac{1}{6} \frac{\partial^3 y}{\partial q^3} \right]_{(q_m, p_m)} & y_{03} &= \left[ \frac{1}{6} \frac{\partial^3 y}{\partial p^3} \right]_{(q_m, p_m)} \\
y_{21} &= \left[ \frac{1}{2} \frac{\partial^3 y}{\partial q^2 \partial p} \right]_{(q_m, p_m)} & y_{12} &= \left[ \frac{1}{2} \frac{\partial^3 y}{\partial q \partial p^2} \right]_{(q_m, p_m)}
\end{aligned} \tag{62}$$

The Taylor's series expansion is generated at the point  $(q_m, p_m)$ . Now, let  $z(y)$  be one of the solutions  $Z_1, Z_2, Z_3$  or  $Z_4$ . We then make a Taylor's series expansion of  $z(y)$

$$z(y) = z_0 + z_1(y - y_m) + \frac{1}{2} z_2(y - y_m)^2 + \frac{1}{6} z_3(y - y_m)^3 \tag{63}$$

where  $y_m$  is the point where the series is generated. When we insert (60) into (63) we get after a very tedious calculation that the stationary point  $t_a^* = z(y)$  is a polynomial function of the two variables  $\omega_a$  and  $\omega_r$ , hence, the decomposed phase function of fifth-order (DTF5) can be written as

$$\begin{aligned}
\varphi_{DTF5}(t_a^*) &= kC_{00} + \varphi_{AZC5}(\omega_a) + \varphi_{RCM5}(\omega_r, \omega_a) + \\
&\varphi_{SRC5}(\omega_r, \omega_a) + \varphi_{HIGH5}(\omega_r, \omega_a)
\end{aligned} \tag{64}$$

$$\begin{aligned}
\varphi_{AZ5}(\omega_r, \omega_a) &= \sum_{n=1}^3 (kC_{0n} - T_n) \omega_a^n + (kC_{0n} - T_6) \omega^4 + \\
&k \sum_{n=5}^{15} C_{0n} \omega_a^n
\end{aligned} \tag{65}$$

$$\begin{aligned}
\varphi_{RCM5}(\omega_r, \omega_a) &= \left[ (-c^{-1}C_{00}) + (kC_{11} - c^{-1}C_{01}) \omega_a + \right. \\
&(kC_{12} - c^{-1}C_{02} - T_2) \omega_a^2 + \sum_{n=3}^{13} (kC_{1n} - c^{-1}C_{0n}) \omega_a^n \\
&\left. - c^{-1} \sum_{n=14}^{15} (C_{0n}) \omega_a^n \right] \omega_r
\end{aligned} \tag{66}$$

$$\varphi_{SRC5}(\omega_r, \omega_a) = \left[ \begin{aligned} &(-c^{-1}C_{11}) \omega_a + \\ &\sum_{n=2}^{11} (kC_{2n} - c^{-1}C_{1n}) \omega_a^n \\ &- c^{-1} \sum_{n=12}^{13} C_{1n} \omega_a^n \end{aligned} \right] \omega_r^2 \tag{67}$$

$$\begin{aligned}
\varphi_{HIGH5}(\omega_r, \omega_a) &= \left[ (-c^{-1}C_{22}) \omega_a^2 + \sum_{n=3}^9 (kC_{3n} - c^{-1}C_{2n}) \omega_a^n \right. \\
&- \sum_{n=10}^{11} c^{-1} C_{2n} \omega_a^n \left. \right] \omega_r^3 \\
&+ \left[ (-c^{-1}C_{33}) \omega_a^3 + \sum_{n=4}^7 (kC_{4n} - c^{-1}C_{3n}) \omega_a^n + \sum_{n=8}^9 -c^{-1} C_{3n} \omega_a^n \right] \omega_r^4 \\
&+ \left[ \sum_{n=4}^8 (-c^{-1}C_{4n}) \omega_a^n \right] \omega_r^5
\end{aligned} \tag{68}$$

where (65)-(68) correspond to (33)-(36) for the DTF4. The decomposed transfer functions for DTF5 are generated in the same way as for DTF4 in (7). We don't give the expressions for the  $C_{mn}$ -coefficients because they are much more complicated than for the fourth-order case and would take many pages to write down here. However, the equations above have been implemented to do DTF5 processing and the results will be shown in Section III.

## E. Implementation

Fig.1 shows the flow diagram for the DTF4 algorithm. The first box indicates that the raw data are divided into main blocks followed by a 2D FFT on each block. We shall now distribute the decomposed transfer functions in (8) in the boxes in the flow diagram. The complex conjugate of a linear range chirp,  $e^{-j\omega_r^2/2b_2}$ , and the higher order transfer function  $H_{HIGH4}^*(\omega_r, \omega_a, R_m)$  are multiplied with the raw data in the 2-D frequency domain. We use a linear range chirp here, however, the transmitted range signal may be of arbitrary form. Then the secondary range correction,  $H_{SRC4}^*(\omega_r, \omega_a, R_m)$ , and the bulk azimuth compression filter,  $H_{AZ4}^*(\omega_a, R_m)$ , are multiplied in this domain followed by an inverse FFT in range. All of these transfer functions are calculated at the center of the main block,  $R_m$ . We could have done the range cell migration correction in the time domain. However, we want to use the decomposed functions in the frequency domain.

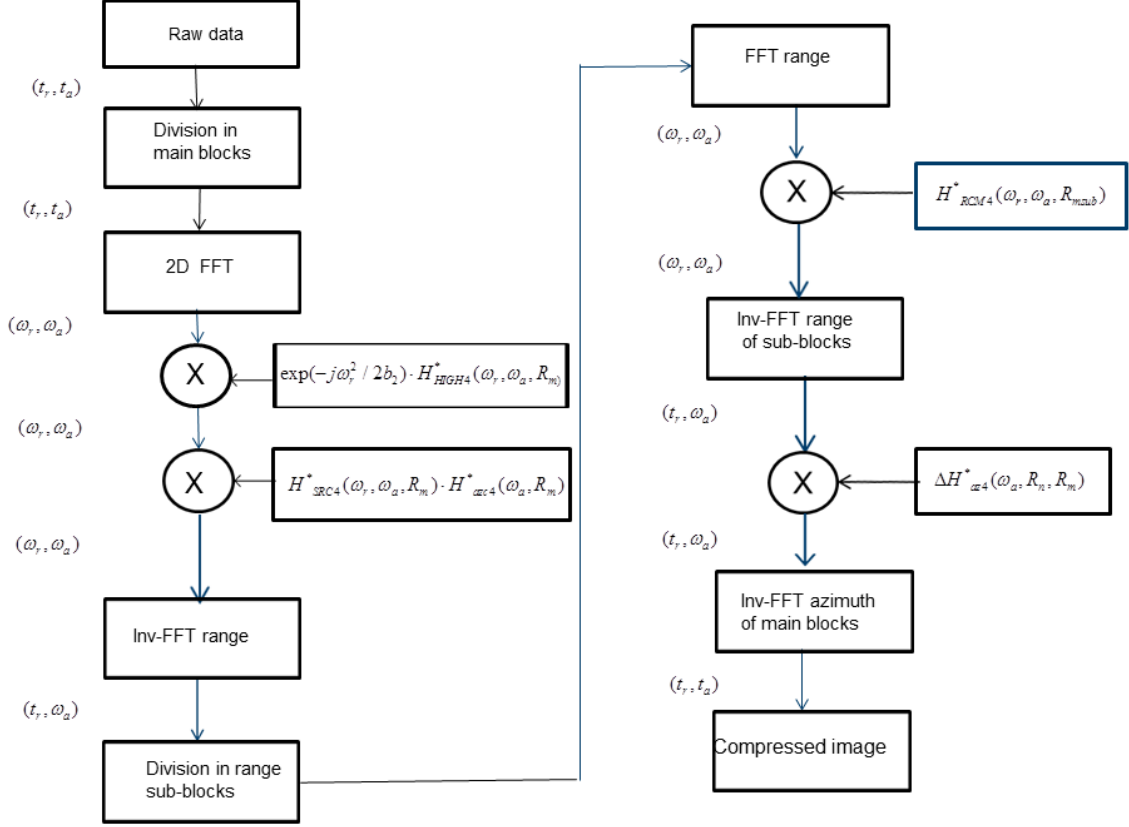


Fig. 1 Flow diagram of the DTF4. The flow diagram for DTF5 is the same with 4 replaced by 5.

We have selected an implementation with division of the main blocks into sub-blocks in range. Division into sub-blocks may not be necessary for a SAR that is yaw steered with small Doppler centroid variations. This increases the processing speed. The division into main blocks and sub-blocks is dependent on SAR parameters, especially the squint, and is not easy to calculate by a simple formula. A study of the point target responses as we do in Section III is preferable. We do a forward FFT and then multiply by the range cell migration correction transfer function,  $H_{RCM4}^*(\omega_r, \omega_a)$ . Then the inverse range FFT is taken of all sub-blocks. The residual azimuth compression

$\Delta H_{az4}^*(\omega_a, R_n, R_m)$ , is now performed for all azimuth lines in the main block. We calculate the azimuth transfer function at  $R_m$  and at range  $R_n$  on both sides of the center in the main block. The residual azimuth compression filter is the given by

$$\Delta H_{az4}^*(\omega_a, R_n, R_m) = H_{az4}^*(\omega_a, R_n) H_{az4}(\omega_a, R_m) \quad (69)$$

Finally, an inverse azimuth FFT is performed in each line in the main block. For the DTF5 algorithm we replace  $H_{RCM4}^*(\omega_r, \omega_a)$  with

$H_{RCM5}^*(\omega_r, \omega_a)$ ,  $H_{SRC4}^*(\omega_r, \omega_a)$  with  $H_{SRC5}^*(\omega_r, \omega_a)$  and so on.

When faster update of Doppler parameters is required at high squint, it may be advantageous to execute the secondary range correction, the bulk azimuth compression and the higher order terms correction in the sub-blocks where range cell migration correction is done. This shows that the decomposition of the transfer function makes a good flexibility to select the best implementation method depending on how Doppler parameters need to be updated.

### III. SIMULATION EXAMPLES

We simulate raw data point targets as described in [7]. The simulations here are done for a monostatic SAR, however, simulation for bistatic SAR can be done as in [7]. TABLE I shows the SAR parameters used in the simulations here. The algorithm is a generic algorithm, it can be implemented for stripmap, sliding spotlight or staring spotlight. We therefore use a complex PRF slightly larger than the azimuth bandwidth as is usual for stripmap processing. If the algorithm

should be used for spotlight processing, merging of several azimuth spectra is needed since the PRF is much lower. We denote the different looks: look -1, look 0 and look 1. The total length of 3 looks is 10.2 s. TABLE II shows the Kepler elements for the orbit used in the simulations. We do simulations for two cases, one with quite small Doppler centroids at low squint at  $yaw = 0.3^\circ$

( $pitch = 0.0^\circ$ ,  $roll = 0.0^\circ$ ) and one case with higher squint and large Doppler centroid at  $yaw = 7.5^\circ$ .

The definition of the attitude reference system used in the simulation can be found in reference [19] in [5]. The five Doppler parameters are shown in TABLE III and TABLE IV for the two cases in the corners of a block with 1000 range x 1000 azimuth pixels. ( $Az=1, Ra=1$ ) is near range early azimuth corner, ( $Az=1000, Ra=1$ ) is near range late azimuth. We can see that the Doppler centroid  $f_1$  changes 4.96 Hz from near to far range in the block in TABLE III and 112.42 Hz in TABLE IV. The large Doppler centroid variation in range is the main reason for division in sub-blocks to do range cell migration correction. We also note that all odd Doppler parameters,  $f_1$ ,  $f_3$  and  $f_5$  have higher

values at higher squint. The  $f_5$  parameter is included in DTF5 and therefore performs better than DTF4 at higher squint as we shall demonstrate later. In both cases we see that all Doppler parameters change only slightly from early azimuth to late azimuth. In order to concatenate sub-blocks in range direction and azimuth blocks in azimuth direction exactly we can perform the azimuth and range stretch operations described in [7].

Fig. 2 shows a 3-look DTF5 processing of a block with size 1000 range x 1000 azimuth pixels and 9 point targets PT1-PT9. PT5 is in the center of the main block and 5 sub-blocks are used here for performing range cell migration correction. TABLE V shows the mean and standard deviations of the quality parameters of the 9 PTs. The mean azimuth resolution is 1.29 pixels which corresponds to 0.34 m. We have used Hamming window with coefficient 0.7 and then the theoretical azimuth resolution is given by ground speed of the beam divided by the azimuth bandwidth.

TABLE I SAR parameters used in the simulations for a monostatic case .

RF-center frequency (GHZ)	9.6
Range chirp bandwidth (MHz)	300
Sampling frequency (MHz)	370
PRF(Hz)	26700
Azimuth filter length 1 look (s)	3.4
Azimuth filter length 3 looks (s)	10.2

TABLE II The Kepler elements for the orbit of the SAR.

$a$ : Semimajor axis (m)	6886008
$i$ : Inclination ( $^\circ$ )	98.0
$e$ : Eccentricity	0.001
$\omega$ : Argument of perigee ( $^\circ$ )	90.0
$\Omega$ : Ascending node ( $^\circ$ )	0.0
$M$ : Mean anomaly ( $^\circ$ )	270.07

TABLE III The five Doppler parameters for  $yaw = 0.3^\circ$  for X-band SAR in the corners of the block processed here of size with size 1000 x 1000 pixels.

$Az$	$Ra$	$Range(m)$	$f_1(s^{-1})$	$f_2(s^{-2})$	$f_3(s^{-3})$	$f_4(s^{-4})$	$f_5(s^{-5})$
1	1	548880.04	244.73	-6357.386	-0.04095	0.57604	-0.00001198
1000	1	548880.46	244.76	-6357.379	-0.04095	0.57605	-0.00002425
1	1000	549284.83	249.69	-6352.549	-0.04217	0.57474	-0.000011819
1000	1000	549285.26	249.72	-6352.542	-0.04217	0.57475	-0.000024348

TABLE IV The five Doppler parameters for  $\text{yaw} = 7.5^\circ$  for X-band SAR in the corners of the block processed here with size 1000 x 1000 pixels.

$Az$	$Ra$	$Range(m)$	$f_1(s^{-1})$	$f_2(s^{-2})$	$f_3(s^{-3})$	$f_4(s^{-4})$	$f_5(s^{-5})$
1	1	548880.53	21293.16	-6344.671	-5.7511	0.56910	0.001284
1000	1	548880.96	21293.19	-6344.664	-5.7511	0.56911	0.001271
1	1000	549285.33	21405.58	-6339.708	-5.7728	0.56774	0.001287
1000	1000	549285.76	21405.61	-6339.701	-5.7727	0.56776	0.001273

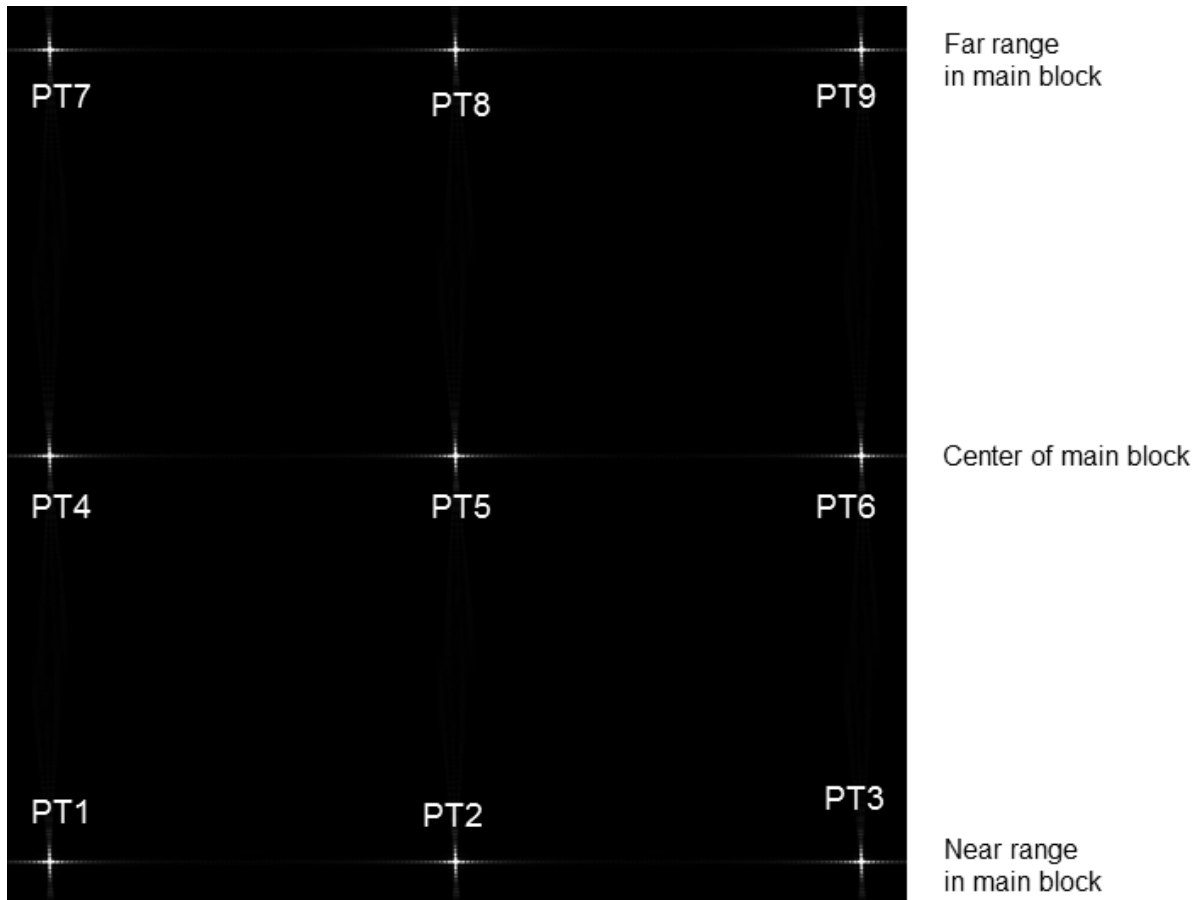


Fig. 2 3 look DTF5 processing of one main block 1000 x 1000 pixels showing 9 point targets.

TABLE V Quality parameter measurements of point targets in Fig.2 processed with DTF5

	Peak amplitude	ISLR (dB)	Azimuth res (pixels)	Range res (pixels)	Err pos Az(pixels)	Err pos Ra(pixels)
mean	19418	-16.00	1.29	1.25	-0.003	-0.01
stdev	256.6	0.19	0.04	0.01	0.066	0.024

In this case the theoretical azimuth resolution is  $7098 \text{ m/s} / (6355 \text{ Hz/s} * 3.4 \text{ s}) = 0.33 \text{ m}$ . The measured and theoretical range resolution is

0.51 m and 0.50 m, respectively. If we had real data we could make 9 looks to get an azimuth resolution approximately equal to the ground range resolution and reduce speckle. The mean azimuth error

position of the nine PTs is  $-0.003$  pixels and the standard deviation is only  $0.066$  pixels, which means that all pixels are very well positioned compared to the position of the point targets in the raw data. The range positions are also very well positioned with one one hundredth of a pixel size accuracy.

Fig. 3A shows PT2 and PT5 with EETF5 processing of the outer look -1. The quality parameters are given in TABLE VI. The peak amplitude of PT2 which is near the block boundary is  $18426$ . This is  $94.1\%$  of PT5 which is in the center of the block. The

azimuth and range resolutions of PT2 are both degraded compared to PT5. The azimuth resolution is increased  $5.6\%$  and the range resolution  $9.5\%$ . DTF4 processing yields practically the same image quality as DTF5 for look -1 and is shown in Fig 3B where 5 sub-blocks in range are used in the processing. There is only a small difference between the quality numbers of PT5 and PT2 as shown in TABLE VII. Fig 3C shows 3-look processing and 5 sub-blocks in range with either DTF5 or DTF4. The quality parameters of PT2 and PT5 are almost the same in TABLE VII and TABLE VIII. These examples show that DTF

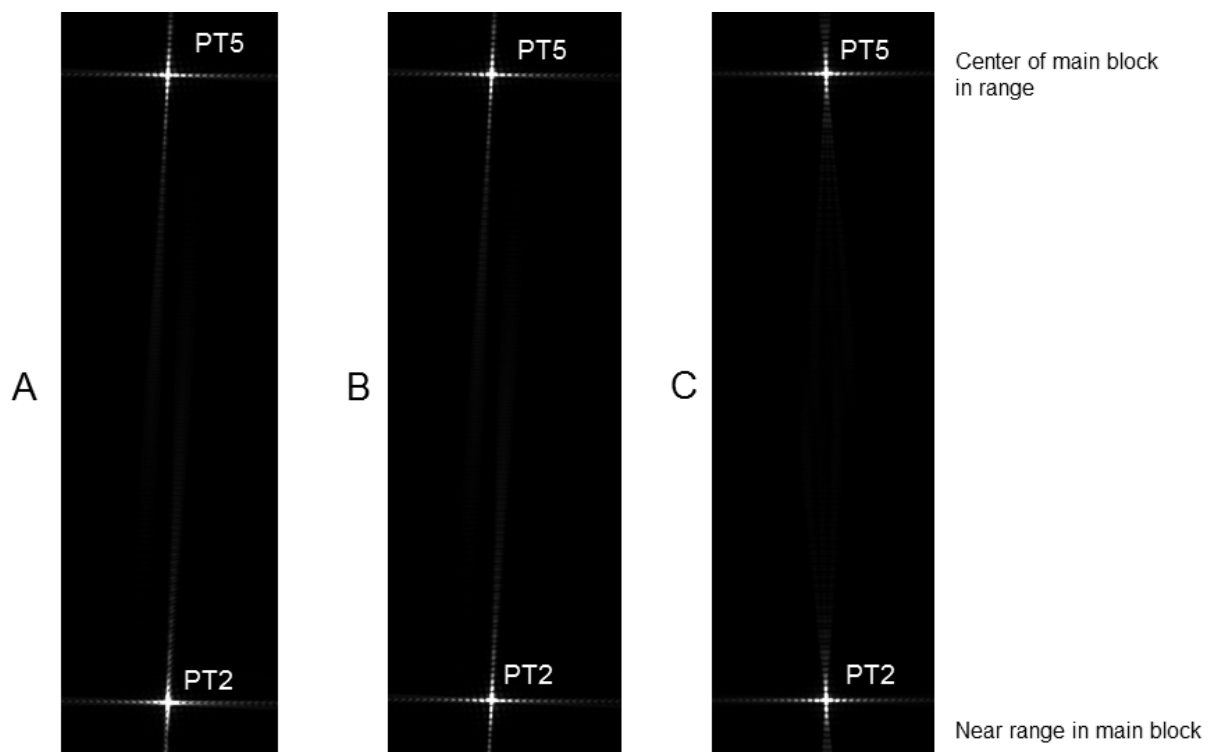


Fig. 3 EETF and DTF processing of point targets PT2 and PT5 at  $yaw = 0.3^\circ$ . Image A: EETF5 look -1. Image B: DTF5, DTF4 look -1. Image C: DTF5, DTF4 3 looks.

TABLE VI Quality parameter measurements of point target PT2 and PT5 Fig. 2 which are zoomed in Fig. 3A. Processing with EETF5.

	Peak amplitude	ISLR (dB)	Azimuth res (pixels)	Range res (pixels)	Err pos Az(pixels)	Err pos Ra(pixels)
PT5	19568	-15.14	1.25	1.26	0.04	-0.01
PT2	18426	-15.79	1.32	1.38	-0.02	-0.62

TABLE VII Quality parameter measurements of point targets in Fig. 3B. DTF4 or DTF5 processing of look -1 using 5 sub-blocks in range.

	Peak amplitude	ISLR (dB)	Azimuth res (pixels)	Range res (pixels)	Err pos Az(pixels)	Err pos Ra(pixels)
PT5	19573	-15.16	1.25	1.26	0.03	-0.01
PT2	19398	-15.53	1.27	1.29	0.00	-0.06

TABLE VIII Quality parameter measurements of point targets in Fig. 3C.3-look processing with DTF4 or DTF5 and 5 sub-blocks in range.

	Peak amplitude	ISLR (dB)	Azimuth res (pixels)	Range res (pixels)	Err pos Az(pixels)	Err pos Ra(pixels)
PT5	19542	-16.05	1.27	1.25	0.00	0.01
PT2	19532	-15.91	1.26	1.27	0.01	-0.03

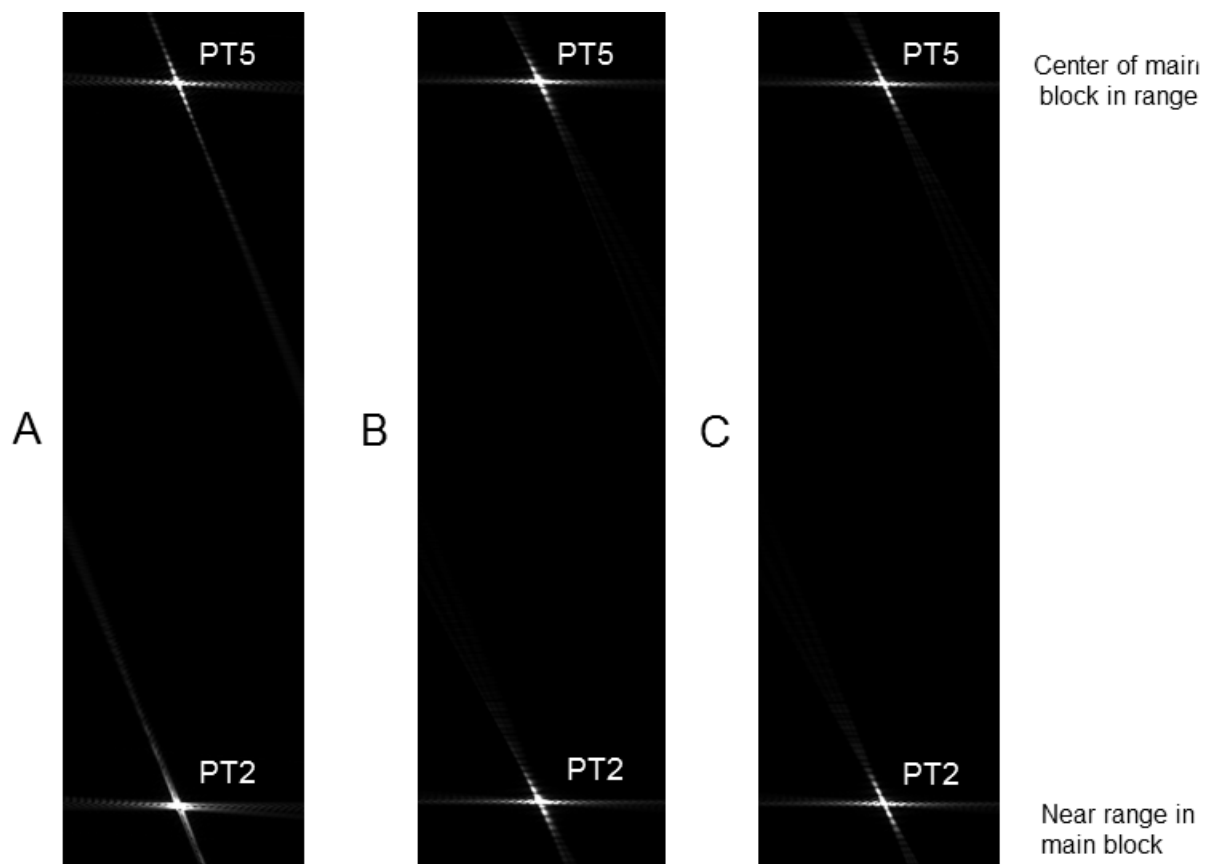


Fig. 4 EETF and DTF processing of point targets PT2 and PT5 at  $yaw = 7.5^\circ$ . Image A: EETF5 look -1. Image B: DTF4 3-look. Image C: DTF5 3-look.

processing improves the quality compared to EETF at  $yaw = 0.3^\circ$ . Furthermore, the measured azimuth resolution is  $(1.26 * 7098 / 26700) = 0.33$  m for DTF4 and DTF5 processing which is the same as the theoretical resolution (see calculation above) to mm

accuracy. The same is found for the range resolution.

Fig. 4 shows the processing of PT2 and PT5 at  $yaw = 7.5^\circ$ . Fig. 4A shows the point targets processed with EETF5 for look -1. The quality parameters are given in TABLE IX. We

can see that the peak amplitude of PT2 is substantially reduced compared to PT5 (15318/19410=78.9 %). The processing with DTF5 for look -1 and 1 sub-block in range is quite similar to that of EETF5 look -1. The peak amplitude for PT5 is 19499 and that for PT2 is 15145. This means that the sub-block processing in the DTF5 improves the quality. The azimuth resolution is degraded from 1.28 pixels to 1.52 pixels and the range resolution is degraded from 1.16 to 1.57 pixels. Fig. 4B shows the point targets processed with 3-look DTF4. The quality parameters are given in TABLE X. The peak amplitudes of both targets are reduced to about 15500 and the azimuth resolution reduced to 1.78 pixels. Fig. 4C shows processing with the DTF5. The quality parameters are given in TABLE XI. Now, the peak amplitudes of both point targets are around 19500 which is almost the same as

processing at  $\gamma_{aw} = 0.3^\circ$  in Fig. 3C. The azimuth resolution is also almost the same as in Fig. 3C (TABLE VIII). These examples show that DTF5 processing achieves the same quality parameters as the theoretically calculated quality parameters, while DTF4 yields substantially reduced quality at this squint. The point target near the block boundary (PT2) is severely blurred using the EETF5, as is shown in TABLE IX.

It has been shown above that the quality parameters of point targets within one main block using DTF5 is very good for the low squint and high squint case. However, we do a final test to check the quality of a point target exactly on the corners of four adjacent main blocks and also adjacent sub-blocks. PT9 is the same target as in Fig. 2. Fig. 5A shows the block boundaries between four adjacent main blocks (az1,ra1), (az2,ra1), (az1,ra2) and (az2,ra2).

TABLE IX Quality parameter measurements of point targets in Fig.4A. Look -1 processing with EETF5.

	Peak amplitude	ISLR (dB)	Azimuth res (pixels)	Range res (pixels)	Err pos Az(pixels)	Err pos Ra(pixels)
PT5	19410	-15.78	1.28	1.16	0.13	0.09
PT2	15318	-16.69	1.52	1.57	0.85	-1.41

TABLE X Quality parameter measurements of point targets in Fig.4B. 3-look processing with DTF4 and 10 sub-blocks in range.

	Peak amplitude	ISLR (dB)	Azimuth res (pixels)	Range res (pixels)	Err pos Az(pixels)	Err pos Ra(pixels)
PT5	15518	-15.21	1.78	1.22	0.40	-0.01
PT2	15523	-14.96	1.77	1.21	0.63	-0.01

TABLE XI Quality parameter measurements of point targets in Fig. 4C. 3-look processing with DTF5 and 10 sub-blocks in range.

	Peak amplitude	ISLR (dB)	Azimuth res (pixels)	Range res (pixels)	Err pos Az(pixels)	Err pos Ra(pixels)
PT5	19490	-16.37	1.27	1.18	0.02	-0.01
PT2	19597	-15.87	1.24	1.16	0.12	0.02

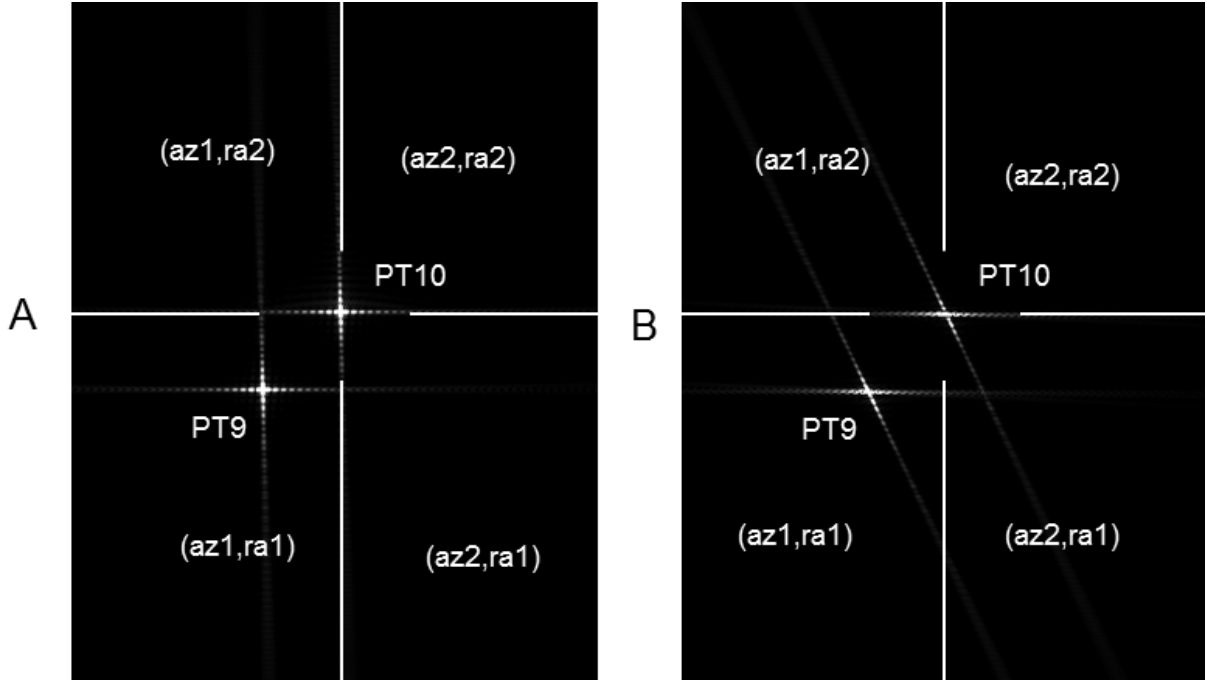


Fig. 5. Point targets P9 and P10 processed with DTF5. Image A: look 0 ,  $yaw = 0.3^\circ$  , Image B: look 0 ,  $yaw = 7.5^\circ$  .

TABLE XII Quality parameter measurements of point targets in Fig. 5A. Block boundaries between blocks (az1,ra1), (az2,ra1), (az1,ra2) and (az2,ra2) are shown. Processing of look 0 with DTF5.

	Peak amplitude	ISLR (dB)	Azimuth res (pixels)	Range res (pixels)	Err pos Az(pixels)	Err pos Ra(pixels)
PT9	19837	-15.74	1.22	1.24	0.09	0.03
PT10	19856	-15.60	1.22	1.24	0.10	0.03

TABLE XIII Quality parameter measurements of point targets in Fig. 5B. Block boundaries between blocks (az1,ra1), (az2,ra1), (az1,ra2) and (az2,ra2) are shown. Processing of look 0 with DTF5.

	Peak amplitude	ISLR (dB)	Azimuth res (pixels)	Range res (pixels)	Err pos Az(pixels)	Err pos Ra(pixels)
PT9	19278	-16.84	1.27	1.21	-0.01	-0.01
PT10	19631	-17.55	1.24	1.17	0.05	0.02

Point target PT10 is the processed target at the common point of the four corners. Fig. 5A and 5 B show processing for  $yaw = 0.3^\circ$  and  $yaw = 7.5^\circ$  , respectively. The quality parameters for Fig. 5A are given in TABLE XII and those for Fig 5.B are given in TABLE XIII. We see that for both for  $yaw = 0.3^\circ$  and for  $yaw = 7.5^\circ$  that the quality of the point target PT 10 in the common point of the corners is almost the same as for PT 9.

#### IV. NOVEL PROPERTIES OF THE DTF ALGORITHM

The EETF4/EETF5 algorithms are based on analytical solutions to the SPA problem using non-hyperbolic phase functions. All operations except for the azimuth compression are done by a single 2D filter. This makes the algorithms degrade with increasing squint due to larger variation of the Doppler parameters, especially the Doppler

centroid. The range cell migration correction was embedded in one 2D filter and small blocks were required for larger squint angles. The decomposition of the transfer function made in [8] inspired the decompositions made in DTF4/DTF5. In [8] they avoided the SPA by using the MSR method with a fourth-order phase function that was approximated from a hyperbolic phase function. Furthermore, they removed the linear range cell migration when doing the MSR. Hence, for the first time the SPA for a non-hyperbolic azimuth phase function has been solved here using a fifth-order polynomial. Furthermore, for the first time both the DTF4 and the DTF5 have been decomposed in analytical expressions. It is then possible to study the degradations of each of the decomposed functions when Doppler parameters are invariant. Especially, the range cell migration and the secondary range cell migration correction can be updated more frequently at demanding geometry which means increasing squint angle.

Until recently, the hyperbolic azimuth phase history has been sufficient for processing of spaceborne SAR data. The RDA, CSA and MWA algorithms mentioned in the introduction make use of the hyperbolic phase functions since a simple solution exists for solving the SPA problem. The staring spotlight SAR processing algorithm in [4] computes the correction to a hyperbolic range history by using numerical methods. The TerraSAR-X satellite is totally yaw steered, which keeps the both the Doppler centroid and its variation very small. The CSA algorithm is therefore still effective because this algorithm may use only one block in range. However, a numerical approach for generation of 2D filters may slow down the algorithm. Since TerraSAR-X is yaw steered the DTF4 algorithm could be implemented as a staring spotlight processing algorithm using subapertures as is done in [4]. When the Doppler centroid variation is small, large blocks can be used. The DTF algorithms may be less efficient than the CSA algorithm for low squint, however, for squints with large Doppler centroid variations in range, the CSA may be less suitable than the DTF algorithms. In [10] they concluded that the CSA algorithm may not be particularly suitable at large squint. Furthermore, the DTF algorithms can have a general range chirp form, while the standard CSA is based on linear chirp. Finally, it should be mentioned that the DTF algorithms will be less efficient with increasing squint and Doppler

parameter variations because blocks need to be reduced in size in range. In addition, the azimuth blocks size must be increased with higher accuracy.

In the future we may expect more clusters of SAR satellites. Interesting for target recognition would be to use several satellites to look at the same area simultaneously with different look and squint angles. The DTF algorithm could be a candidate for processing of images with resolution of a few decimeters at large squint. Although the analytical calculation of the DTF filters is quite cumbersome for a person, the efficiency may be very good compared to numerical computation of filters. The precision of the processing using DTF4 or DTF5 should be an advantage at higher squint.

## V. CONCLUSIONS

A new algorithm, called DTF tailored for spaceborne SAR processing, taking into account nonhyperbolic phase history at large integration times, has been developed, implemented, and tested. The DTF has been calculated fully analytically using the stationary phase approximation by solving fourth-order (DTF4) and fifth-order (DTF5) polynomial equations followed by Taylor's series expansion of the stationary point solution for decomposition of the phase function. The DTF4 yields high quality point target responses at low squint with 3-look azimuth resolution 0.3 m while the DTF5 has to be used at larger squint with large Doppler centroid variations. The algorithm is well suited for parallel computation and has been implemented using OpenMP in Windows.

## APPENDIX A. T-COEFFICIENTS OF THE DTF4

It can be shown that the  $T$  coefficients in (30) are given by

$$\begin{aligned}
 T_0 = & y_0 - y_1 x_m + \frac{1}{2} y_2 x_m^2 - \frac{1}{6} y_3 x_m^3 + y_1 x_1 + \frac{1}{2} y_2 x_1^2 \\
 & - y_2 x_m x_1 + \frac{1}{6} y_3 x_1^3 - \frac{1}{2} y_3 x_m x_1^2 + \frac{1}{2} y_3 x_m^2 x_1
 \end{aligned} \tag{70}$$

$$T_1 = y_1 x_2 - y_2 x_m x_2 + \frac{1}{2} y_3 x_1^2 x_2 - y_3 x_m x_1 x_2 + \quad (86)$$

$$y_2 x_1 x_2 + \frac{1}{2} y_3 x_m^2 x_2 \quad (71)$$

$$T_2 = y_1 x_3 + y_2 x_1 x_3 - y_2 x_m x_3 + \frac{1}{2} y_3 x_1^2 x_3 - y_3 x_m x_1 x_3 + \frac{1}{2} y_3 x_m^2 x_3 \quad (72)$$

$$T_3 = \frac{1}{2} y_2 x_2^2 + \frac{1}{2} y_3 x_1 x_2^2 - \frac{1}{2} y_3 x_2^2 x_m \quad (73)$$

$$T_4 = y_2 x_2 x_3 + y_3 x_1 x_2 x_3 - y_3 x_m x_2 x_3 \quad (74)$$

$$T_5 = \frac{1}{2} y_2 x_3^2 + \frac{1}{2} y_3 x_1 x_3^2 - \frac{1}{2} y_3 x_m x_3^2 \quad (75)$$

$$T_6 = \frac{1}{6} y_3 x_2^2 \quad (76)$$

$$T_7 = \frac{1}{2} y_3 x_2^2 x_3 \quad (77)$$

$$T_8 = \frac{1}{2} y_3 x_2 x_3^2 \quad (78)$$

$$T_9 = \frac{1}{6} y_3 x_3^3 \quad (79)$$

#### APPENDIX B. C-COEFFICIENTS OF THE DTF4

$$C_{00} = 2(c_1 T_0 + c_2 T_0^2 + c_3 T_0^3 + c_4 T_0^4) \quad (80)$$

$$C_{01} = 2(c_1 T_1 + 2c_2 T_0 T_1 + 3c_3 T_0^2 T_1 + 4c_4 T_0^3 T_1) \quad (81)$$

$$C_{02} = 2 \left( c_1 T_3 + c_2 T_1^2 + 2c_2 T_0 T_3 + 3c_3 T_0^2 T_3 + 3c_3 T_0 T_1^2 + 4c_4 T_0^3 T_3 + 6c_4 T_0^2 T_1^2 \right) \quad (82)$$

$$C_{03} = 2 \left( c_1 T_6 + 2c_2 T_1 T_3 + 2c_2 T_0 T_6 + c_3 T_1^3 + 3c_3 T_0^2 T_6 + 6c_3 T_0 T_1 T_3 + 4c_4 T_0^3 T_6 + 4c_4 T_0 T_1^3 + 12c_4 T_0^2 T_1 T_3 \right) \quad (83)$$

$$C_{04} = 2 \left( c_2 T_3^2 + 2c_2 T_1 T_6 + 3c_2 T_1^3 T_3 + 3c_3 T_0 T_3^2 + 6c_3 T_0 T_1 T_6 + c_4 T_1^4 + 6c_4 T_0^2 T_3^2 + 12c_4 T_1^2 T_6 + 12c_4 T_0 T_1^2 T_3 \right) \quad (84)$$

$$C_{05} = 2 \left( 2c_2 T_3 T_6 + 3c_3 T_1^2 T_6 + 3c_3 T_1 T_3^2 + 6c_3 T_0 T_3 T_6 + 4c_4 T_1^3 T_3 + 12c_4 T_0^2 T_3 T_6 + 12c_4 T_0 T_1^2 T_6 + 12c_4 T_0 T_1 T_3^2 \right) \quad (85)$$

$$C_{06} = 2 \left( 2c_2 T_6^2 + c_3 T_3^3 + 3c_3 T_0 T_6^2 + 6c_3 T_1 T_3 T_6 + 4c_4 T_1^3 T_6 + 4c_4 T_0 T_3^3 + 6c_4 T_0^2 T_6^2 + 6c_4 T_1^2 T_3^2 + 24c_4 T_0 T_1 T_3 T_6 \right) \quad (86)$$

$$C_{07} = 2 \left( 3c_3 T_3^2 T_6 + 3c_3 T_1 T_6^2 + 4c_4 T_1 T_3^3 + 12c_4 T_1^2 T_3 T_6 + 12c_4 T_0 T_3^2 T_6 + 12c_4 T_0 T_1 T_6^2 \right) \quad (87)$$

$$C_{08} = 2 \left( 3c_3 T_3 T_6^2 + c_4 T_3^4 + 6c_4 T_1^2 T_6^2 + 12c_4 T_1 T_3^2 T_6 + 12c_4 T_0 T_3 T_6^2 \right) \quad (88)$$

$$C_{09} = 2(c_3 T_6^3 + 4c_4 T_3^3 T_6 + 4c_4 T_0 T_6^3 + 12c_4 T_1 T_3 T_6^2) \quad (89)$$

$$C_{0,10} = 2(4c_4 T_1 T_6^3 + 6c_4 T_3^2 T_6^2) \quad (90)$$

$$C_{0,11} = 2(4c_4 T_3 T_6^3) \quad (91)$$

$$C_{0,12} = 2(c_4 T_6^4) \quad (92)$$

$$C_{11} = 2(c_1 T_2 + 2c_2 T_0 T_2 + 3c_3 T_0^2 T_2 + 4c_4 T_0^3 T_2) \quad (93)$$

$$C_{12} = 2(2c_2 T_1 T_2 + 6c_3 T_0 T_1 T_2 + 12c_4 T_0^2 T_1 T_2) \quad (94)$$

$$C_{13} = 2 \left( 2c_2 T_2 T_3 + 3c_3 T_1^2 T_2 + 6c_3 T_0 T_2 T_3 + 12c_4 T_0^2 T_2 T_3 + 12c_4 T_0 T_1^2 T_2 \right) \quad (95)$$

$$C_{14} = 2 \left( 2c_2 T_2 T_6 + 6c_3 T_0 T_2 T_6 + 6c_3 T_1 T_2 T_3 + 4c_4 T_1^3 T_2 + 12c_4 T_0^2 T_2 T_6 + 24c_4 T_0 T_1 T_2 T_3 \right) \quad (96)$$

$$C_{15} = 2 \left( 2c_3 T_2 T_3^2 + 6c_3 T_1 T_2 T_6 + 12c_4 T_1^2 T_2 T_3 + 12c_4 T_0 T_2 T_3^2 + 24c_4 T_0 T_1 T_2 T_6 \right) \quad (97)$$

$$C_{16} = 2 \left( 6c_3 T_2 T_3 T_6 + 12c_4 T_1^2 T_2 T_6 + 12c_4 T_1 T_2 T_3^2 + 24c_4 T_0 T_2 T_3 T_6 \right) \quad (98)$$

$$C_{17} = 2(3c_3 T_2 T_6^2 + 4c_4 T_2 T_3^2 + 12c_4 T_0 T_2 T_6^2 + 24c_4 T_1 T_2 T_3 T_6) \quad (99)$$

$$C_{18} = 2(12c_4 T_2 T_3^2 T_6 + 12c_4 T_1 T_2 T_6^2) \quad (100)$$

$$C_{19} = 2(12c_4 T_2 T_3 T_6^2) \quad (101)$$

$$C_{1,10} = 2(4c_4 T_2 T_6^3) \quad (102)$$

$$C_{22} = 2(3c_2 T_2^2 + 3c_3 T_0 T_2^2 + 6c_4 T_0^2 T_2^2) \quad (103)$$

$$C_{23} = 2(3c_3 T_1 T_2^2 + 12c_4 T_0 T_1 T_2^2) \quad (104)$$

$$C_{24} = 2(3c_3 T_2^2 T_3 + 6c_4 T_1^2 T_2^2 + 12c_4 T_0 T_2^2 T_3) \quad (105)$$

$$C_{25} = 2(3c_3 T_2^2 T_6 + 12c_4 T_0 T_2^2 T_6 + 12c_4 T_1 T_2^2 T_3) \quad (106)$$

$$C_{26} = 2(6c_4 T_2^2 T_3^2) \quad (107)$$

$$C_{27} = 2(12c_4 T_2^2 T_3 T_6) \quad (108)$$

$$C_{28} = 2(6c_4 T_2^2 T_6^2) \quad (109)$$

$$C_{33} = 2(2c_3 T_2^3 + 4c_4 T_0 T_2^3) \quad (110)$$

$$C_{34} = 2(4c_4 T_1 T_2^3) \quad (111)$$

$$C_{35} = 2(4c_4 T_2^3 T_3) \quad (112)$$

$$C_{36} = 2(4c_4 T_2^3 T_6) \quad (113)$$

$$C_{44} = 2(4c_4 T_2^4) \quad (114)$$

## ACKNOWLEDGMENT

The author wishes to thank Norwegian Defence Research Establishment (FFI) for giving the opportunity to do this interesting investigation of spaceborne SAR processing. Thanks to Research Manager Richard B. Olsen at FFI and the anonymous reviewers for giving valuable comments to the manuscript.

## REFERENCES

- [1] Eldhuset, K: Ultra high resolution spaceborne SAR processing. *IEEE Transactions on Aerospace and Electronic Systems*, **40**, 1 (July 2004), 370-378.
- [2] Wu, Y., Sun, G-C., Yang, C., Yang, J., Xing, M., Bao, Z. Processing of Very High Resolution Spaceborne Sliding Spotlight SAR Data Using Velocity Scaling, *IEEE Transactions on Geoscience Remote Sensing*, **54**, 6 (March 2016), 1505-1518.
- [3] Wang, P., Liu, W., Chen, J., Niu, M., Yang, W. A High-Order Imaging Algorithm for High-Resolution Spaceborne SAR Based on a Modified Equivalent Squint Range Model, *IEEE Transactions on Geoscience Remote Sensing*, **53**, 3 (March 2015), 1225-1235.
- [4] Prats-Iraola, P., Scheiber, R., Rodriguez-Cassola, M., Mittermayer, J., Wollstadt, S., De Zan, F., Bräutigam, B., Schwerdt, M., Reigber, A., Moreira, A. On the Processing of Very High Resolution Spaceborne SAR Data. *IEEE Transactions on Geoscience Remote Sensing*, **52**, 10 (October 2014), 6003-6016.
- [5] Eldhuset, K. A New Fourth-Order Processing Algorithm for Spaceborne SAR. *IEEE Transactions on Aerospace and Electronic Systems*, **34**, 3 (July 1998), 824-835.
- [6] Kim, D.H., Lim, B.G., Lee, D.H., Yoon, J.C., Yang, D.C., Jung, H., R. (2016) SAR processing by a modified CSA based algorithm with a delicate azimuth matched filter ETF4ZDT. In *Proceedings of EUSAR 2016*, Hamburg, Germany, June 6-9, 2016, 174-177.
- [7] Eldhuset, K. Spaceborne Bistatic SAR Processing Using the EETF4 Algorithm. *IEEE Geoscience and Remote Sensing Letters*, **6**, 2 (April 2009), 194-198.
- [8] Neo, Y.L., Wong, F.H., and Cumming, I.G. Processing of Azimuth-Invariant Bistatic SAR Data Using the Range Doppler Algorithm. *IEEE Transactions on Geoscience Remote Sensing*, **46**, 1 (January 2008), 14-21.
- [9] Luo, Y., Zhao, B., Han, X., Wang, R., Song, H., Deng, Y. A Novel High-Order Range Model and Imaging Approach for High-Resolution LEO SAR, *IEEE Transactions on Geoscience Remote Sensing*, **52**, 6 (June 2014), 3473-3485.
- [10] Imperatore, P., Pepe, A., Lanari, R. Spaceborne Synthetic Aperture Radar Data Focusing on Multicore-Based Architectures. *IEEE Transactions on Geoscience Remote Sensing*, **54**, 8 (August 2016), 4712-4731.
- [11] Bennet, J.R., Cumming, I. and Deane, R. (1980) The digital processing of SEASAT synthetic aperture radar data. In *Proceedings of the IEEE International Radar Conference, April 1980*, 168-175.
- [12] Raney, K., Runge, H., Bamler, R., Cumming, I.G., and Wong, F. (1994) Precision SAR processing using chirp scaling. *IEEE Transactions on Geoscience and Remote Sensing*, **32**, 4 (July 1994), 786-799.
- [13] Bamler, R. (1992) A comparison of range-Doppler and wavenumber domain SAR focusing algorithms. *IEEE Transactions on Geoscience and Remote Sensing*, **30**, 4 (July 1992), pp1-pp2.
- [14] [Online]. Available: <http://mathworld.wolfram.com/QuarticEquation.html>
- [15] Rottmann, K. (1960) *Mathematische Formelsammlung*. Mannheim: Bibliographisches Institut AG, 1960.



**Knut Eldhuset** was born in 1958 and received the cand. scient. degree (M.Sc.) in nuclear physics in 1983 from the University of Oslo and the dr. scient. degree (Ph.D.) in physics/signal processing (1987) from the University of Tromsø. He has been with the Norwegian Defence Research Establishment (FFI) since 1983, working on processing and applications of satellite Synthetic Aperture Radar (SAR) data. His research interests cover a wide range of topics, including orbit simulation, geolocation, automatic ship detection, SAR/scanSAR processing, InSAR processing, scattering theory, polarimetry, MTI simulations and processing of bi-static SAR data. His results have contributed to numerous national projects, to European defence research projects and to several studies for the European Space Agency. He has developed advanced algorithms for ship and wake detection, and for SAR processing using the Extended Exact Transfer Function (EETF), both of which were developed into commercial products by the Kongsberg Group. While his early work was focused on ERS, ENVISAT and Radarsat-1, his more recent work has focused on polarimetric analysis of Radarsat-2 images and InSAR combined with stereoSAR using TerraSAR-X/TanDEM-X and COSMO-SkyMed for DEM generation.